Characterising *in vivo* acoustic cavitation during lithotripsy with time-frequency methods

K B Cunningham, A J Coleman, T G Leighton and P R White

Ultrasound has many applications in clinical therapy [1]. These range from the commonplace, where the patient is probably unaware of the involvement of acoustics, such as dental ultrasonic scalers and drills, to the experimental, such as for tumour therapy. Applications include the unexpected, such as phonophoresis, where ultrasound assists the absorption of drugs through the skin. Perhaps the most common use is for physiotherapy, a survey as long ago as 1985 suggesting over a million treatments per year in England and Wales. It employs frequencies of 1-3 MHz, in continuous-wave or pulsed modes. The duration of each pulse, and separation between them, is typically a few milliseconds. The acoustic pressure amplitudes employed in physiotherapy are up to about 1 MPa (10 bar; 214 dB re 20 μPa; 240 dB re 1 μPa).

A completely different sound field is used in lithotripsy, where pulses of only a few microseconds duration are separated by 'quiet periods' of around a second, and contain shocks with peak positive pressures of up to 100 MPa (1000 bar). Several thousand such shocks are directed onto unwanted gall, kidney or salivary stones, in order to break them up into fragments small enough to be naturally expelled. The exact mechanism for stone destruction is under continued debate [2] the two contenders being direct effects from stress waves induced in the stone, and indirect effects from acoustic cavitation. The ubiquitous generation of cavitation by lithotripsy has important implications.

The object of therapeutic ultrasound is to change tissue or physiology. This is in complete contrast to diagnostic ultrasound (see the companion paper in this issue [3]), which ideally should bring about no tissue change. The mandate for the use of therapeutic ultrasound is that the beneficial effects must be judged to outweigh any detrimental effects the treatment might also produce on the body. This is a particularly salient point for therapeutic ultrasound. This is because, in addition to tissue heating, which is relatively well understood and controllable, the other major mechanism by which therapeutic ultrasound operates is ultrasonic cavitation, a phenomenon with a reputation for being difficult to measure and control [4].

Therefore it is extremely important to measure the occurrence of *in vivo* cavitation in humans. However, the generation of such a destructive phenomenon *in vivo*, for the purposes of research, poses difficult, even insurmountable, moral and ethical issues. Lithotripsy offers a unique opportunity, because *in vivo* cavitation is being generated anyway, and is available for study. The development of devices and techniques to study ultrasonic cavitation *in vivo*, as described in this paper, serves not only the study of lithotripsy, but is a unique opportunity to gain fundamental information basic to the safe use of both therapeutic and diagnostic ultrasound.

This paper describes how acoustics can be used passively and non-invasively to monitor the cavitation that occurs *in vivo* in humans during lithotripsy.

Shock wave lithotripsy treatment

Shock wave lithotripters create and focus shock pulses on stones within the body using a system as shown in *Figure 1*. Photographs of two Dornier clinical lithotripsy systems are shown in *Figure 2*. A shock wave is initiated external to the body through an electrical discharge of a capacitor across an electromagnetic transducer, a spark gap, or an array

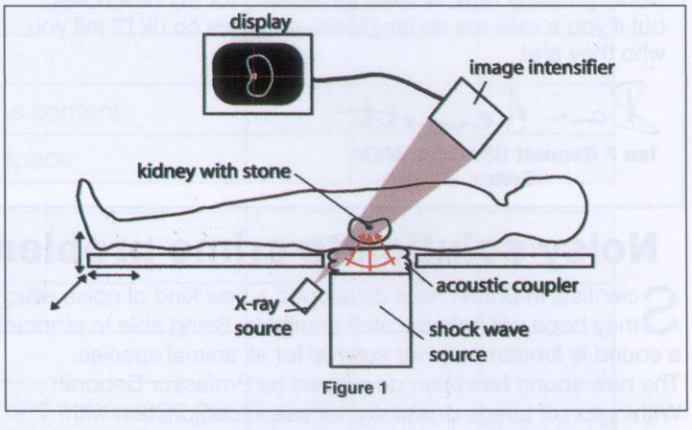

Figure 1. **A typical shock wave lithotripsy system for treating kidney stones.**

of piezoelectric elements. Geometrical acoustic principles are used to focus the wavefronts, which propagate through an aqueous acoustic medium that couples to the patient. Treatment begins with alignment of the acoustic focal region with the target using X-ray or ultrasonic imaging to locate the stone. The operator may adjust the amplitude of the shock waves. For example, the output setting on the Storz lithotripter, which is used in this study, may be varied on an arbitrary scale from 1 to 9. Patients experience varying degrees of pain and may be sedated or anaesthetised. Alignment of the target and lithotripter focal region is periodically verified and updated by the operator.

Modelling cavitation in lithotripsy

Cavitation refers to the phenomenon whereby microscopic bubbles undergo extensive growth in response to excitation by an acoustic field. This

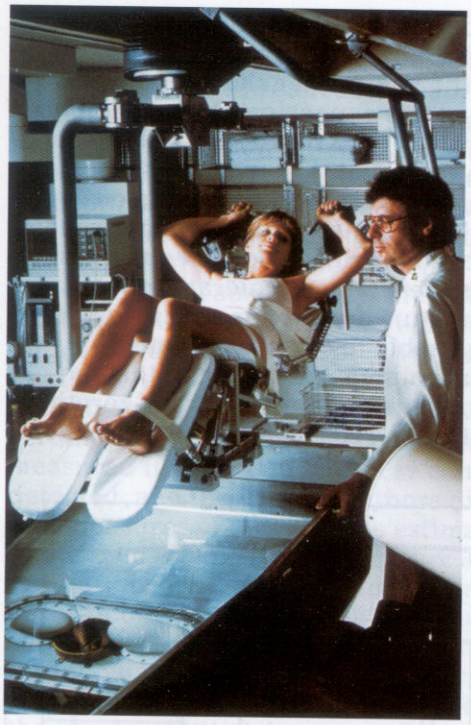

Figure 2. (a)

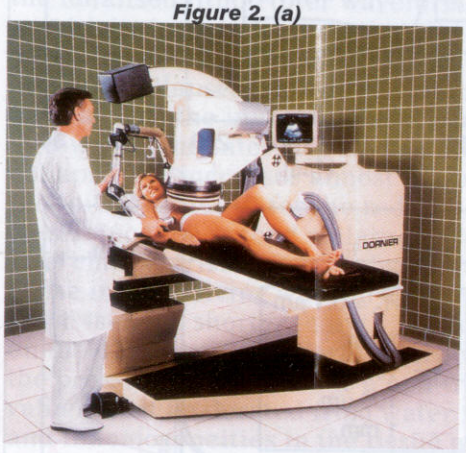

Figure 2. (b)

Figure 2. (a) **The original Dornier HM3 clinical lithotripter. (b) The Dornier MPL9000. Perhaps the most obvious difference between the two is the way they couple the shockwave (generated by a 20 kV underwater discharge) into the tissue. In (a) the patient is lowered into a large water bath into which the voltage is discharged. In (b) no immersion is necessary: the shock system is contained within a separate water-filled unit, the front membrane of which is pressed against the skin.**

is followed by a rapid collapse of these bubbles that can result in the formation of microjets, which can be extremely erosive, an effect implemented in ultrasonic cleaning baths [see **Ref. 5**, in this issue]. Shock waves are emitted when the bubble rebounds. To a first approximation, the bubble gas behaves isothermally during growth, but adiabatically during collapse. Hence the compressed gas can attain transient temperatures of several thousand degrees. Whilst these are important for some sonochemical effects **[5]**, it is the rebound shocks and microjets which play a greater part in stone fragmentation.

Acoustic cavitation is most easily studied in the laboratory, where it can be visible to the naked eye and where it is possible to measure physical effects such as sonoluminescence, erosion, and acoustic emissions **[Ch. 5 of Ref. 6]**. For *in vivo* observations cavitation can be characterised by passive monitoring of acoustic signals emanating from within the body. Analysis of these signals in the time-frequency (TF) domain provides greater detectability over analysis in the time domain alone.

Cavitation during lithotripsy is commonly modelled using the Gilmore-Akulichev equation that

continued on page 12

Characterising *in vivo* acoustic cavitation during lithotripsy with time-frequency methods

continued from page 11

describes the radial motion of a single spherical bubble in an infinite medium as it is driven by an acoustic field [7]. The advantage of the Gilmore model is that it incorporates the compressibility of the liquid, and allows the prediction of the pressure pulses emitted by the bubble on rebound. It is these pulses that form the basis of non-invasive detection of cavitation *in vivo*.

The assumptions inherent in this model are particularly interesting in relation to lithotripsy: the bubble remains spherical at all time, and the gas homogeneous, with the result that the presence of gas shocks and liquid microjets, which may be extremely important for stone fragmentation, are not included. Indeed the model ignores any interactions with solids, obviously crucial for stone fragmentation (see for example *Figure 5.57* of **Ref. 6**). Whilst simulations which are capable of incorporating microjets, gas shocks, and solid bodies have been developed [8], the Gilmore-Akulichev model will be used here. This is because it most readily predicts the far field acoustic emission resulting from cavitation, and it is these emissions which are to be exploited in this paper for remote characterisation of cavitation.

The Gilmore-Akulichev model also requires the existence of a free-floating microscopic spherical bubble to 'seed' the cavitation event. Once cavitation has occurred, such nuclei are likely to be plentiful. However the threshold for cavitation (on which clinical safety guidelines are based) depends on the size distribution of bubble seeds that naturally occur *in vivo*. This distribution is not known. Therefore, lithotripsy studies give us a unique opportunity to establish characteristics of this population. Such information would be invaluable in estimating the likelihood of unwanted and potentially hazardous cavitation during diagnostic ultrasonic procedures such as foetal scanning.

An idealised pressure waveform at the focus of a lithotripter is shown in the inset in *Figure 3a*. A positive peak of high amplitude, up to 100 MPa, and short rise time, approximately 100 ns, is followed by a tensile tail of peak negative magnitude down to -10 MPa, the duration of the entire pulse being of several microseconds [9]. The bubble radius time history, calculated for various initial bubble radii, is shown in *Figure 3a*. The lithotripter shock reaches the bubble at time $t = 0$. In the first few microseconds, the positive pressure of the incident pulse causes a decrease in the bubble size because the compressibility of the gas is much less than that of the surrounding liquid. We will call this the 'zeroth' bubble collapse. It occurs for the bubble having initial radius $R_0 = 100\ \mu m$ at time $t = 4\ \mu s$ (*Figure 3a*, red trace).

After this, the negative tail of the driving waveform initiates an expansion phase of the bubble, which continues after the driving pulse has passed because of the inertia of the moving fluid (here until more than 200 μs after the lithotripter shock first meets the bubble). During this expansion phase, which is of much greater duration than the driving lithotripter pulse, the bubble radius may increase by several orders of magnitude (note that the abscissa on *Figure 3a* is on a logarithmic scale). As a maximum radius is approached the decreased pressure inside the bubble causes the wall to accelerate inwards again. Fluid momentum during this ensuing collapse phase causes the bubble to compress to much less than its initial volume. We shall call this the 'first collapse'. It occurs at time t_1 after the zeroth collapse (so that for the red trace in *Figure 3b*, the

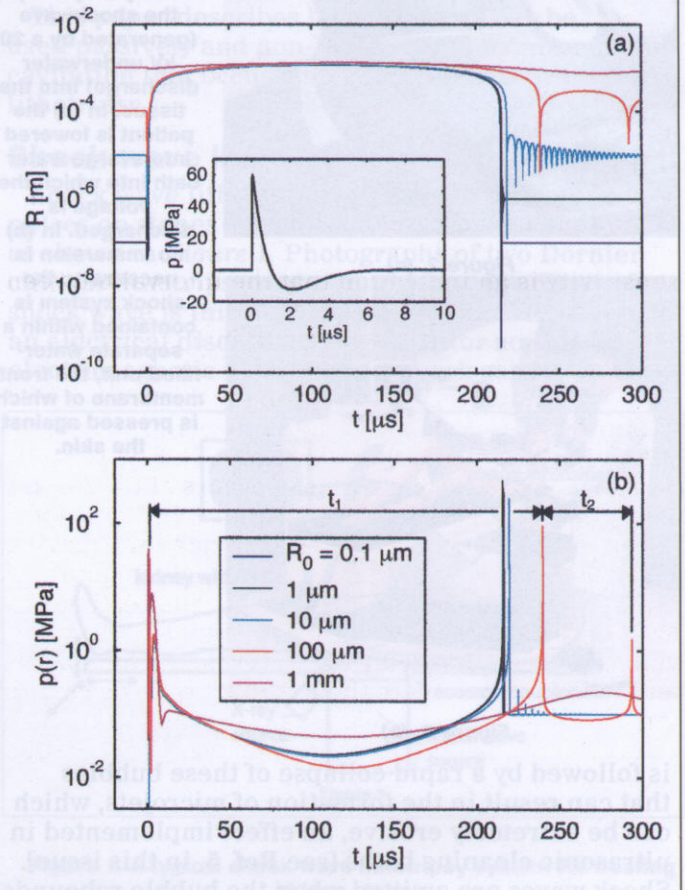

Figure 3

Figure 3. **Calculated response of bubbles of various initial radii, to a typical lithotripter pulse (inset). The figure shows (a) the radius as a function of time, and (b) the corresponding acoustic emissions at r = 1.5 mm from the bubble centre.**

first collapse occurs at time $t = 239\ \mu s$, giving an interval from the zeroth collapse of $t_1 = 235\ \mu s$).

As the bubble rebounds from this 'first collapse', a spherically diverging shock front is emitted. It has sufficient amplitude for remote detection. All the bubbles in *Figure 3a* (except for the one whose initial radius, at 1 mm, is too large to give significant expansion or collapse) show high internal pressures, indicative of the launch of rebound shocks, simultaneous with the minimum bubble radius attained at the end of the 'first collapse' (at time $200\ \mu s < t < 250\ \mu s$ in *Figure 3b*).

In practice, instabilities are likely to prevent the bubble remaining spherical for the entire

collapse phase and fragmentation of the bubble as it approaches a minimum radius is likely. Bubble fragmentation will reduce the amplitude of expected acoustic emissions, and seed the liquid with more nuclei for subsequent driving pulses. The model, which assumes no fragmentation, predicts that the first collapse will be followed by several rebounds and collapses of decreasing magnitude, and indeed this can occur even in the presence of fragmentation **[10]**. Simply because of the scale of the drawing, the multiple collapses are most clearly seen in the trace for an initial bubble size of $R_0 = 10\ \mu$m (*Figure 3b*, light blue trace).

To summarise, t_1 is the time interval between the zeroth and first collapse events. This can be directly measured if the rebound shocks can be remotely detected, and the current authors did hypothesise that measures of t_1 could give estimations of the size of the seed bubbles (note in *Figure 3b* how the high pressure peaks corresponding to the first collapse occur in order of increasing seed bubble radius, R_0) **[11]**. However the simulations in water for various initial bubble radii indicate a weak dependence of t_1 on the initial bubble radius when subject to the idealised lithotripter waveform. This lack of sensitivity is an indication that the interval between detection of the rebound emissions from the zeroth and first collapses (t_1) is not a suitable parameter for determining the initial bubble radius.

However, the interval between the first and second collapses (t_2) increases almost in direct proportion to the initial radius (t_2 for the red trace in *Figure 3b* is 53 μs, since the second collapse occurs at $t = 292\ \mu$s). This characteristic time is also almost independent of the initial driving waveform, provided the driving pulse is much shorter than t_1. This weak dependence on the driving pulse is fortuitous because estimating the pressure field *in vivo* is a non-trivial matter; values must be derated from water measurements and inhomogeneities in the tissue must be accounted for. Thus, if a second collapse occurs, and the time interval t_2 can be measured, we have a robust method for estimating the bubble radius.

Figure 4. **Example of the effect of gas diffusion on bubble dynamics for bubbles of various initial radii. The driving pulse is the same as for Figure 3.**

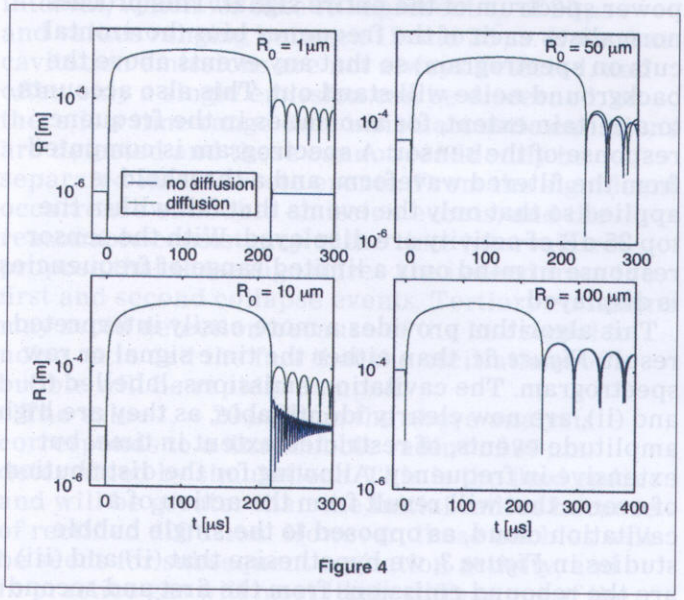

Figure 4

An additional effect of importance, if we are to consider t_2 to be our key indicator of bubble size, is rectified diffusion **[6]**. This phenomenon occurs when dissolved gas in the surrounding liquid diffuses into the bubble while it is in the greatly expanded state (ie. during the interval t_1). At this time the gas inside the bubble is at a greatly reduced concentration compared with its initial value. This forces dissolved gas in the surrounding liquid to come out of solution and enter the bubble. The result of including diffusion into the calculations is shown in *Figure 4*. For the smallest value of initial radius considered, $R_0 = 1\ \mu$m, the effect is most noticeable. Specifically, both the final radius of the bubble, and the time period for the rebounds, increase because of the extra mass of gas inside the bubble. The effect of diffusion decreases with an increase in the initial radius, and at $R_0 = 100\ \mu$m this effect is negligible. This observation can be explained as follows. Bubbles with a smaller initial radius tend to undergo a much greater relative change in size. Therefore when they attain maximum radius (which is similar for all R_0 values **[6]**), the gas concentration inside the bubble will be much lower and diffusion more encouraged.

The size of the bubble nucleus which seeds cavitation in humans *in vivo* is currently not known, yet is a necessary input parameter into the models on which the guidelines for the safe exposure levels for diagnostic ultrasound are made **[12, 13]**. Hence this study of lithotripsy, a therapy, will provide for the first time information necessary to the assessment of safe levels for diagnostic ultrasound. As stated above, the size of the bubble nucleus, which seeds cavitation, can be determined from the interval between the first and second collapses (t_2). As *Figure 3b* shows, a pressure pulse is emitted at the moment of each collapse. The object of this paper is the acoustic detection of these rebound pulses, and from their timing, to estimate the size of the bubble nuclei present *in vivo*.

However, this requires detection of rebound emissions within the *in vivo* acoustic field up to a millisecond after the passage through the target area of the lithotripter pulse. The *in vivo* acoustic field can be assumed to consist of a complex juxtaposition of the incident shock pulse, scattered and reverberant fields, and the emissions from cavitation events. The constraining effects of tissue on bubble growth are also of consequence, as the size of nephrons within the kidneys is on the order of 1 mm, *ie.* a similar size to the maximum expected bubble radii calculated in *Figure 3a*. Additionally, the cavitation signals are not from a single bubble, but a cloud. Nevertheless, the Gilmore model provides a useful benchmark for comparisons with measured data, and provides physical insight into trends in cavitation. The acoustic field, monitored from outside the body, has signals separated in time with frequency characteristics, making time-frequency (TF) methods ideal. An analysis of *in vivo* data from clinical trials is now presented.

In vivo measurements

For clinical measurements a non-invasive system is implemented to measure cavitation activity in the focal zone of the lithotripter. A piezoceramic

continued on page 14

Characterising *in vivo* acoustic cavitation during lithotripsy with time-frequency methods

continued from page 13

spherical 'bowl' of diameter 10 cm and resonant frequency 1 MHz is aligned confocally with the lithotripter and acoustically coupled to the patient [11]. A schematic of this arrangement is shown in *Figure 5*. The receiver is most sensitive to emissions originating in its focal region, which is cigar-shaped and approximately 5 mm long by 3 mm wide. This type of receiver has high sensitivity, but relatively poor bandwidth. Thus, a frequency analysis is only expected to provide useful results over a limited range, and for most results presented we will limit ourselves to a 100% bandwidth from 0.5 to 1.5 MHz.

A measured waveform is shown in *Figure 6a*. The signal is a combination of the scattered incident field, scattered reverberations, and the emissions of possibly many bubbles, which is why the signal is not as clean as that from predictions such as in *Figure 3b*. Additionally, ringing is apparent because of the finite bandwidth of the transducer. The signal from the scattered incident lithotripter pulse is evident starting at time $t = 0$, labelled (i) in the plot. Between $t = 250$ and 300 μs a couple of pressure spikes (events) are registered, labelled (ii) and (iii).

Although there are events of similar or greater magnitude earlier in the time-history, previous experience [11] allows us to make an *a priori* identification of these as cavitation rebound emissions. This is a somewhat subjective task when considering data such as this. Confirmation may be obtained by analysing signals in the TF domain,

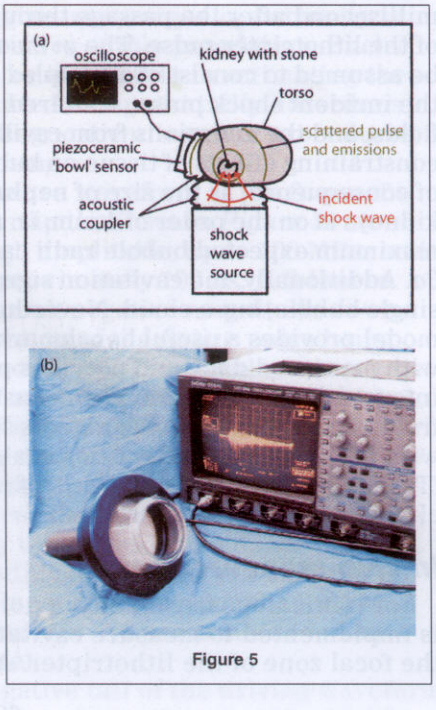

Figure 5

Figure 5. **Schematic of the set-up for clinical measurements. (a) The figure shows a cross-section through the human torso, containing a kidney. In contact with that torso is the lithotripter and, aligned confocally with this, the passive detector. Its purpose is to detect acoustic signals originating in the vicinity of the stone. (b) The photograph shows the detector, its housing containing a curved 10 cm diameter piezoceramic transducer. The detection trace on the oscilloscope resembles Figure 6a.**

since cavitation is characterised by broadband radiation (resulting from the impulse-like nature of the rebound shocks). Hence, we can identify cavitation events from a change in the time varying power spectrum.

A spectrogram of the signal, *Figure 6b*, is calculated using a short time Fourier transform [14]. The amplitudes are mapped on a logarithmic (decibel) scale with an arbitrary reference. There is significant background noise in the low frequency region. This is in part because the initial lithotripter pulse has a fundamental period that relates to approximately 0.25 MHz and the lower frequency reverberations are less quickly dampened. No information is seen for frequencies above 2 MHz because of the bandwidth of the sensor. Cavitation

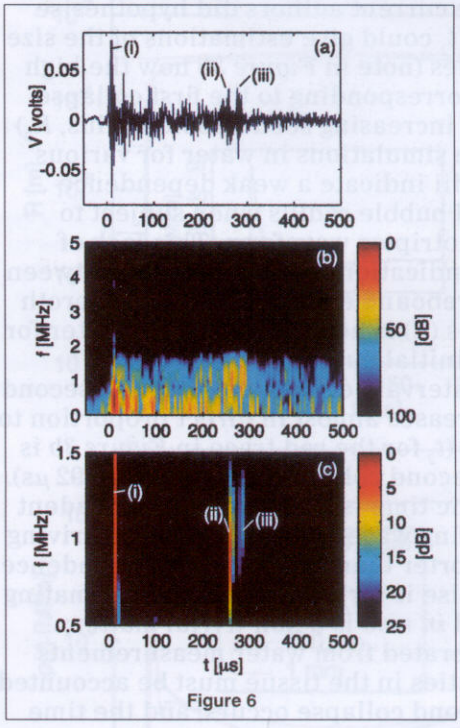

Figure 6

Figure 6. (a) **Pressure waveform at the lithotripter focus. *(b)* The raw spectrogram of this signal. (c) The improved spectrogram after filtering and displaying only the top 25 dB of the dynamic range. Features of the signal are the scattered incident pulse, (i), and the acoustic emissions from cavitation, (ii) and (iii).**

signals in *Figure 6b* are still not obviously identified.

To obtain a more useful TF representation, additional processing is performed. The time series is filtered with a digital filter designed to flatten the power spectrum of the entire signal. This process normalises each of the frequency bins (horizontal cuts on spectrogram) so that any events above the background noise will stand out. This also accounts, to a certain extent, for anomalies in the frequency response of the sensor. A spectrogram is computed from the filtered waveform, and a threshold is applied so that only the events that fall within the top 25 dB of activity are displayed. With the sensor response in mind only a limited range of frequencies is displayed.

This algorithm provides a more easily interpreted result, *Figure 6c*, than either the time signal or raw spectrogram. The cavitation emissions, labelled (i) and (ii), are now clearly identifiable, as they are high amplitude events, of restricted extent in time, but extensive in frequency. Allowing for the distribution of events that will result from the action of a cavitation cloud, as opposed to the single bubble studies in *Figure 3*, we hypothesise that (ii) and (iii) are the rebound emissions from the first and second

collapses respectively. The algorithm described here is applied to all subsequent TF computations.

Figure 7 (left column) shows time waveforms measured in a single patient at different lithotripter discharge settings. The Stortz Modulith SL20 lithotripter used in this study has arbitrary amplitude settings for the operator from 1 to 9, with most patients treated at a maximum setting of 6 or 7. From the waveforms it is possible to identify a cavitation collapse signal at the higher settings, but for the lowest (setting 1) there is a degree of uncertainty.

The spectrograms corresponding to these waveforms, processed as for *Figure 6b*, are plotted in the right column of *Figure* 7. Note that these spectrograms are only plotted over the frequency range 0.5 - 1.5 MHz, which is the frequency range that is most important for this data. From the spectrogram for setting 1 it is apparent that even at this lowest setting cavitation signals are being registered at a time $t \approx 190\ \mu s$ for this patient. The interval between the scatter of the lithotripter pulse ($t = 0$) and the cavitation signals increases with source amplitude. This change in the time of the signals with amplitude reinforces that these are cavitation emissions, and not simply scattered or reverberating pulses.

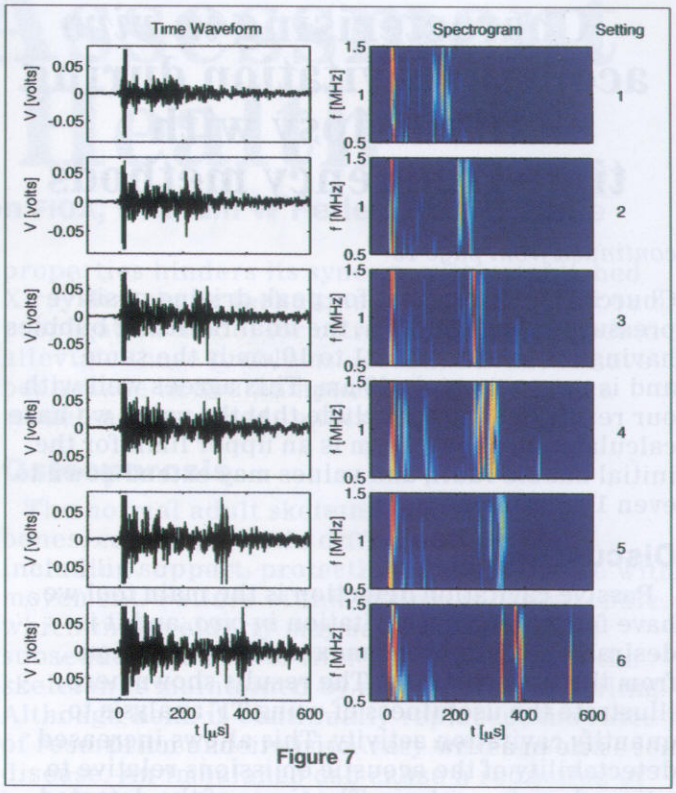

Figure 7. **In vivo acoustic emission waveforms (left column) and their spectrograms (right column). Measurements are for a single patient over a range of lithotripter output settings.**

Preliminary results

In the TF plots of *Figure* 7 for settings 2, 3, and 4 it appears as if two emissions are registered within about 50 μs of each other. This observation leads us to consider the time region around the registration of cavitation emissions in greater detail. Spectrograms of a selection of *in vivo* data, concentrating on the emissions, are shown in *Figure 8*. Note that emissions separated by less than about 10 μs cannot confidently be identified as separate signals because of inadequate time resolution of the TF result.

From the data presented in *Figure 8*, and an analysis of additional data, it was found that when a double emission signature is detected the interval time varies between about 15 and 30 μs. Specifically, from an analysis of 35 recordings, 13 clear double emissions were identified with a mean time interval, which we take to represent t_2, of 20 μs and values ranging between 12 and 35 μs. Note that cavitation emissions are not always detected, and often only a single emission can be discerned, or there is a time range over which acoustic emissions are detected and these cannot confidently be separated into discrete events. From the significant occurrence of double emission events, and the reasonable consistency of the time interval, we propose that these signatures are indeed from the first and second collapse events. Tertiary emissions may avoid detection because of the low signal to noise ratio and the fact that the oscillations of a bubble will be rapidly damped.

The value $t_2 = 20\ \mu s$ from the above analysis corresponds to a final bubble radius of 37 μm, determined by simulations. This is the final radius and will be greater than the initial radius because of rectified diffusion. However, these bubbles will be seeds for subsequent cavitation activity, and in practice gas will most likely diffuse out of the

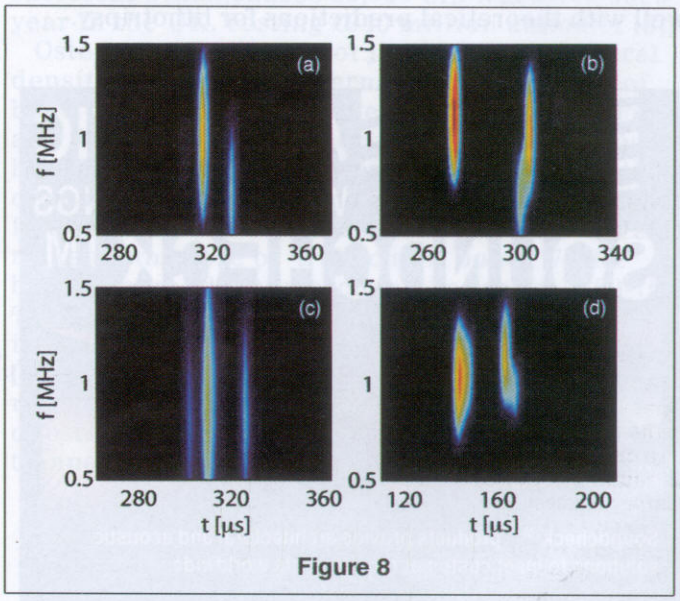

Figure 8. **Spectrograms of data from clinical measurements zooming in on the time region when cavitation emissions are detected. Data for which two distinct emissions are discernible are shown.**

bubbles during the quiet period in-between pulses.

Determination of an initial bubble radius from the final bubble radius is a not a trivial matter though. The increase in the bubble radius, caused by diffusion, depends upon the initial radius and the driving waveform. Numerical simulations have shown a weak dependence of the final radius on the initial radius as the driving waveform amplitude is increased. Specifically, in a numerical study

continued on page 16

Characterising *in vivo* acoustic cavitation during lithotripsy with time-frequency methods

continued from page 15

Church [7] showed that for peak driving positive pressures above 50 MPa, the final radius of bubbles having initial size from 1 to 10 μm is the same, and is approximately 40 μm. This agrees well with our result. We thus conclude that the value we have calculated of about 40 μm is an upper limit for the initial bubble radii, and values may extend down to even 1 micron.

Discussion

Passive cavitation detection is the main tool we have for monitoring cavitation *in vivo*, and it is desirable to extract the maximum information from the data obtained. The results shown here illustrate the usefulness of using TF analysis to quantify cavitation activity. This allows increased detectability of the acoustic emissions relative to a time domain analysis. The times of the detected acoustic emissions can be used to infer a value for the radius of bubbles occurring *in vivo*. A final radius of about 40 μm has been calculated, which agrees well with theoretical predictions for lithotripsy.

Determining the initial radius from this data is beyond the scope of this paper as it requires a greater knowledge of the acoustic driving field *in vivo*, and calculations using this information.

Acknowledgements

The authors would like to thank Dr Prashant Verma for supplying *in vivo* lithotripsy data.

REFERENCES

1. F A Duck, A Baker, and H C Starrit, *Ultrasound in Medicine* (Institute of Physics Publishing, London, 1998).
2. B Sturtevant, in *Smith's Textbook of Endourology*, various editors (Quality Medical Publishing, St. Louis, MO, 1996), pp. 529–592.
3. E R Hughes, T G Leighton, G W Petley, and P R White, Ultrasonic Assessment of Bone Health, *Acoustics Bulletin* (this issue).
4. G R Ter Haar, Biological effects of ultrasound in clinical applications, in *Ultrasound: Its chemical, physical, and biological effects*, edited by K S Suslick (VCH Publishers, New York, 1988).
5. P R Birkin, T G Leighton, Y E Watson, and J F Power, Acoustoelectrochemistry, *Acoustics Bulletin* (this issue).
6. T G Leighton, *The Acoustic Bubble* (Academic Press, London, 1994), §4.3.1(b)(iii), §4.4.3, §5.4.2.
7. C C Church, A theoretical study of cavitation generated by an extracorporeal shock wave lithotripter, *J. Acoust. Soc. Am.* **86**, 215-227, (1989).
8. G J Ball, B Howell, T G Leighton, and M Schofield, Shock-induced collapse of a cylindrical air cavity in water: a Free-Lagrange simulation, *Shock Waves* **10**, 265-276 (2000).
9. A J Coleman and J E Saunders, A survey of the acoustic output of commercial extracorporeal shock wave lithotripters, *Ultrasound Med. Biol.* **15**, 213-227 (1989).
10. T G Leighton, B T Cox, and A D Phelps, The Rayleigh-like collapse of a conical bubble, *J. Acoust. Soc. Am.* **107**, 130-142 (2000).
11. A J Coleman, M J Choi, J E Saunders, and T G Leighton, Acoustic emission and sonoluminescence due to cavitation at the beam focus of an electrohydraulic shock wave lithotripter, *Ultrasound Med. Biol.* **18**, 267-281 (1992).
12. R E Apfel and C K Holland, Gauging the likelihood of cavitation from short-pulse, low-duty cycle diagnostic ultrasound, *Ultrasound Med. Biol.* **17**, 179-185 (1991).
13. C K Holland and R E Apfel, An improved theory for the prediction of microcavitation thresholds, *IEEE Trans. Ultrason. Ferro. Freq. Control* **36**, 204-208 (1989).
14. S Qian and D Chen, *Joint Time-Frequency Analysis*, (Prentice Hall PTR, New Jersey, 1996).

Kevin B Cunningham is a Trainee Clinical Scientist at Guys and St. Thomas' NHS Hospital Trust, London. Andrew J Coleman is Head of the Non-ionising Radiation Section of the Medical Physics Department, Guy's and St. Thomas' NHS Hospital Trust, London. Timothy G Leighton FIOA is Professor of Ultrasonics and Underwater Acoustics, Institute of Sound and Vibration Research, University of Southampton. Paul R White is Senior Lecturer in Underwater Systems, Institute of Sound and Vibration Research, University of Southampton.